

Coupled consolidation analysis of pipe–soil interactions

Santiram Chatterjee, David J. White, and Mark F. Randolph

Abstract: Current design practice for pipe–seabed interaction in soft soils is generally based on the assumption of undrained behaviour throughout laying and subsequent operation. In reality, drainage and consolidation around a partially embedded pipe can have a marked effect on the vertical penetration and horizontal breakout resistance. In this paper, a large-deformation finite element methodology coupled with the “modified Cam clay” plasticity soil model has been developed to study the coupled consolidation behaviour of soil around partially embedded seabed pipelines. Simulations of penetration show that after laying, subsequent consolidation leads to further embedment by an amount dependent on the level of drainage that occurred during laying. Also, if the pipe is embedded under undrained conditions, the waiting period between laying and operation allows the soil around the pipe to consolidate under the pipe self-weight. The consolidation process results in an increase in the strength of the soil. The lateral breakout resistance and the direction of pipe movement on breakout thus depend on the consolidated strength of the soil around the pipe, as well as the applied loading. The envelopes of vertical–lateral combined loading bearing capacity differ markedly from those predicted assuming undrained behaviour throughout.

Key words: pipeline, offshore engineering, clay, consolidation, penetration, finite element method.

Résumé : La pratique courante de conception de l’interaction tuyau-fond marin est généralement basée sur l’hypothèse d’un comportement non drainé durant le placement et durant l’opération subséquente. En réalité, le drainage et la consolidation autour d’un tuyau partiellement enfoui peut avoir un effet marqué sur la pénétration verticale et la résistance horizontale à la séparation. Dans cet article, une méthodologie par éléments finis à grande déformation couplée avec le modèle de plasticité du sol « Cam clay modifié » a été développée pour étudier le comportement couplé en consolidation du sol autour de tuyaux partiellement enfouis dans le fond marin. Des simulations de pénétration montrent que suite à la déposition, la consolidation subséquente entraîne un enfouissement supplémentaire dépendamment du niveau de drainage s’étant produit durant la déposition. De plus, si le tuyau est enfoui en conditions non drainées, la période d’attente entre la déposition et l’opération permet au sol autour du tuyau de consolider sous le poids du tuyau. Le processus de consolidation résulte en une augmentation de la résistance du sol. La résistance à la séparation latérale et la direction du mouvement du tuyau lors de la séparation dépendent ainsi de la résistance à la consolidation du sol autour du tuyau, de même que sur la charge appliquée. Les enveloppes de capacité portante en sollicitations verticales-latérales combinées diffèrent de façon marquée de celles prédites en supposant un comportement non drainé. [Traduit par la Rédaction]

Mots-clés : tuyau, ingénierie en mer, argile, consolidation, pénétration, méthode par éléments finis.

Introduction

When offshore oil and gas reserves are exploited in deep-water, long pipelines are required within each field and are often used to transport the hydrocarbons to shore. In shallow water, where hydrodynamic loading is severe, pipelines are sometimes buried in a trench or secured with alternative stabilization measures. In deeper water, the option of burying the pipe is uneconomical. Deep-water offshore pipelines are laid directly onto the seabed. High operating temperature and pressure result in high axial strains in the pipe, mobilizing axial resistance between the pipe and the soil. Resulting compressive axial forces in the pipe may be relieved by lateral buckling of the pipe at designed locations, where the pipe can move several times its diameter laterally (Bruton et al. 2008).

To design a reliable pipeline that includes such lateral buckling, it is necessary to predict the lateral and axial pipe–soil resistance forces, which both depend on the pipe embedment and the strength of the surrounding soil. In deep water, the seabed typically comprises soft fine-grained sediments, which can consolidate and change in strength over the time periods relevant to the operating life of a pipeline. In this paper, the effects of consolida-

tion on two key aspects of deep-water pipeline design are studied: firstly, the effect of consolidation on pipeline embedment; and secondly, the effect of consolidation on the lateral breakout behaviour.

Undrained embedment and lateral breakout of pipelines have been studied theoretically (Randolph and White 2008), numerically (Aubeny et al. 2005; Merifield et al. 2008, 2009; Wang et al. 2010; Chatterjee et al. 2012a, 2012b) and experimentally (Cheuk et al. 2007; Dingle et al. 2008; Cardoso and Silveira 2010). Theoretical solutions based on limit plasticity have been validated through experimental and numerical studies. Aspects of this work are now used routinely in design to assess the initial embedment of pipelines on clay (White and Cheuk 2005, 2009; AtkinsBoreas 2008). This approach assumes that undrained conditions apply throughout the laying process and subsequent operations, and consolidation settlements are generally neglected. Also, it is usually assumed that the soil strength during pipe breakout is unaffected by consolidation under the pipe weight during the period between laying and breakout. The effect of these assumptions is investigated in this study.

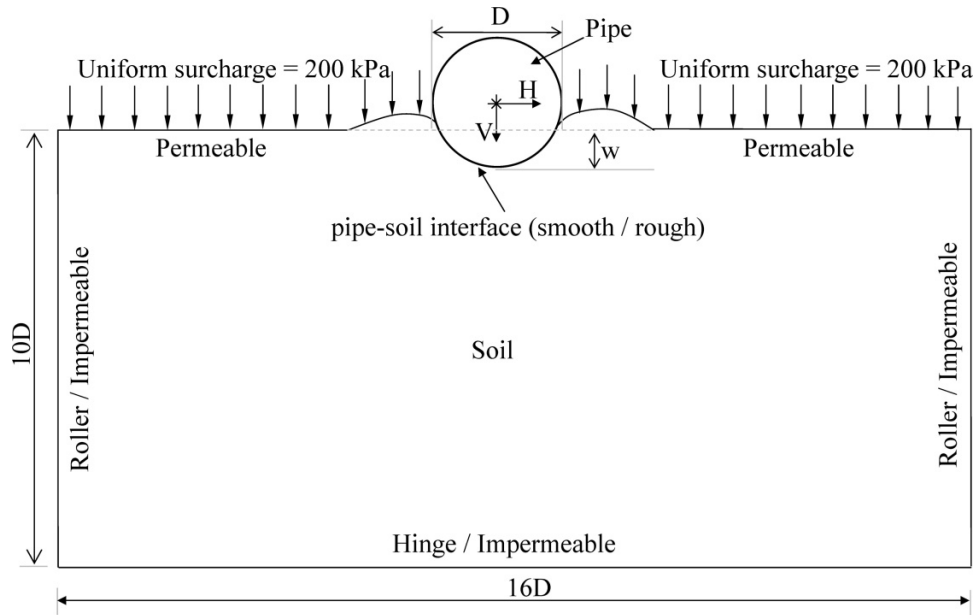
Previous efforts in the literature to model coupled consolidation behaviour under partially embedded pipes have mainly been

Received 16 August 2012. Accepted 1 May 2013.

S. Chatterjee, D.J. White, and M.F. Randolph. Centre for Offshore Foundation Systems – M053, The University of Western Australia, 35 Stirling Highway, Crawley, Perth, WA 6009, Australia.

Corresponding author: David J. White (e-mail: david.white@uwa.edu.au).

Fig. 1. Schematic of the problem studied.



limited to small-strain elastic solutions (Gourvenec and White 2010; Krost et al. 2011). The prediction of pore-water pressure dissipation assuming the soil to be elastic can be reasonably accurate. However, the assessment of settlement associated with consolidation can be erroneous if plastic properties are not taken into account. Chatterjee et al. (2012c) developed a large-deformation finite element (FE) methodology combined with the “modified Cam clay” (MCC) plasticity soil constitutive model to study the pore pressure dissipation beneath partially embedded seabed pipelines. In this paper, the same methodology has been used to study the effect of consolidation on penetration behaviour and subsequent lateral breakout resistance.

Numerical methodology

A large-deformation FE methodology based on the “remeshing and interpolation technique with small strain” (RITSS; Hu and Randolph 1998a, 1998b) and using the ABAQUS commercial FE software (Dassault Systèmes 2011) was developed for this study. The RITSS methodology is a variant of the Arbitrary Lagrangian Eulerian (ALE; Ghosh and Kikuchi 1991) approach of solving large-deformation nonlinear problems. In this method, mesh and material displacements are uncoupled to avoid mesh distortion and entanglement. Large displacement of the pipe is accomplished in several steps by moving the pipe in a series of small displacements and performing a small-strain Lagrangian analysis using ABAQUS in each step. After each small-strain analysis, the boundary of the deformed domain is extracted and the whole soil domain is remeshed.

The MCC soil constitutive model was used to simulate the coupled consolidation behaviour. During each remeshing step, the effective stress, void ratio, pore-water pressure, and current size of the yield envelope (controlled by the pre-consolidation pressure, p'_c) are all remapped from the old mesh to the new mesh. The output parameters that are calculated at integration points — such as effective stress — are first recovered from the old integration points to the old nodes using the superconvergent patch recovery (SPR) method (Zienkiewicz and Zhu 1992) and then interpolated to the new integration points.

For nodal solution parameters, such as pore-water pressure, there is no need for a recovery process. These parameters are interpolated directly from the old nodes to the new nodes. The interpolated parameters are assigned as initial conditions for the

next small-strain step. This process is repeated until the desired pipe displacement is achieved. The whole process is automated by a master FORTRAN program and the different ABAQUS stages are carried out using the in-built scripting language Python (Wang et al. 2010; Chatterjee et al. 2012a).

Model description

A two-dimensional plane strain model was constructed with the pipe as a rigid body and the soil as deformable. The extent of the model was 10 times the pipe diameter in the vertical direction and 8 times the pipe diameter in the horizontal direction on both sides of the pipe. The side boundaries of the model were free to move in the vertical direction, but restrained against horizontal movement. The bottom boundary was fixed, preventing vertical and horizontal movement. Drainage was allowed only at the top soil surface and pore-water flow normal to the pipe-soil interface was prohibited. A schematic diagram of the problem studied and main notation used are shown in Fig. 1.

A very small displacement of 1% of the pipe diameter, D , was applied at the pipe reference point in each step. Six-noded triangular plane strain elements of type CPE6MP within the ABAQUS library were used for discretization of the soil domain. A fine mesh with minimum side length of the triangular elements of $0.02D$ was adopted near the pipe. The extent of the finest meshing from the centre of the pipe at the start of the analysis was up to $1.25D$ on both sides and below from the mudline. Figure 2 shows the FE mesh before any pipe displacement and after the pipe had been penetrated into the soil by half its diameter.

Soil parameters

The MCC soil constitutive model (Roscoe and Burland 1968; Schofield and Wroth 1968) was adopted for this study. The numerical parameters used for all the analyses are listed in Table 1. These are typical properties of the kaolin clay used for experimental research at The University of Western Australia (Stewart 1992). A uniform pressure of 200 kPa was applied at the top soil surface. This alleviates numerical problems associated with the very low shear strength of the soil at the mudline when using the “Cam clay” soil model and normally consolidated conditions (Senthilkumar et al. 2011).

As well as providing numerical stability, this surcharging technique minimizes the variation in soil properties with depth. This

Fig. 2. Finite element meshes before and after pipe penetration: (a) initial mesh; (b) mesh after pipe penetration.

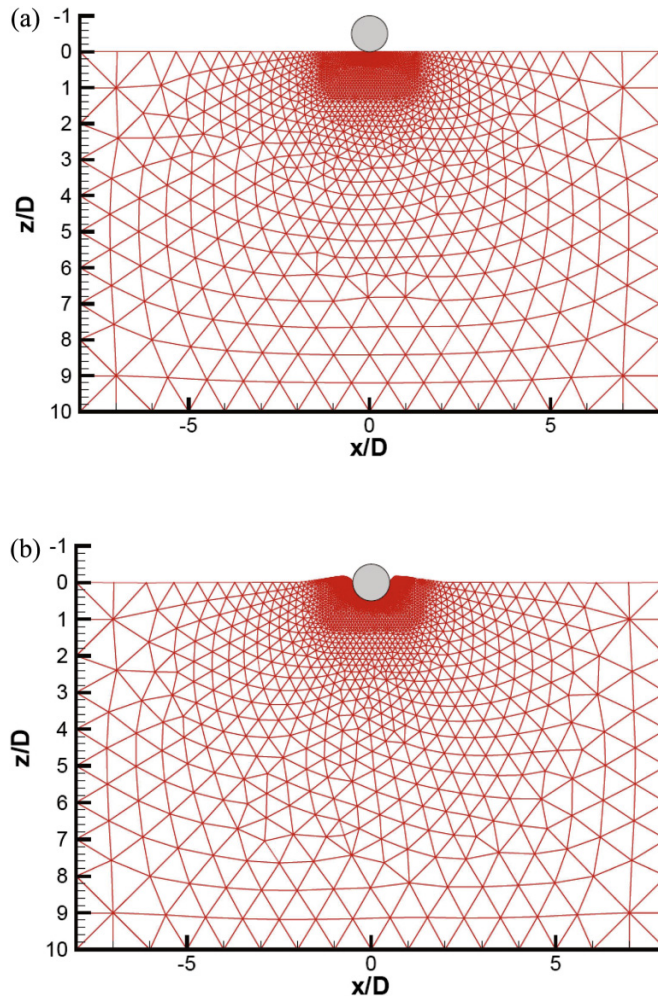


Table 1. Input parameters for numerical study.

Parameters	Values
Slope of critical state line in p' - q space, M (angle of internal friction in triaxial compression, ϕ'_{tc} (°))	0.92 (23.5)
Void ratio at $p' = 1$ kPa on critical state line, e_{cs}	2.14
Slope of normally consolidated line in e - $\ln(p')$ space, λ	0.205
Slope of swelling and recompression line in e - $\ln(p')$ space, κ	0.044
Poisson's ratio, ν	0.3
Saturated bulk unit weight, γ_{sat} (kN/m ³)	15.0
Unit weight of water, γ_w (kN/m ³)	10.0
Permeability of soil, k (m/s)	1.0e ⁻⁹
Diameter of the pipe, D (m)	0.5

Note: p' , mean effective stress; q , deviatoric stress.

makes normalization of the results more straightforward, as properties such as the coefficient of consolidation and the initial undrained shear strength are essentially invariant with depth. The variation in shear strength with depth, often quantified by the relationship $s_{ug}D/s_{um}$, where s_{ug} is the shear strength gradient and s_{um} is the mudline strength intercept, affects the vertical and horizontal soil resistance. Adoption of an artificial surcharge of 200 kPa restricts the study to $s_{ug}D/s_{um}$ of close to zero. However, the main focus here is to evaluate the general trends of response observed as a result of partial consolidation, compared with corresponding results for purely undrained conditions. The soil is

considered to be one-dimensionally (K_0) consolidated, with K_0 given by

$$(1) \quad K_0 = 1 - \sin \phi'_{tc}$$

where ϕ'_{tc} is the angle of internal friction in triaxial compression.

The initial effective stress state at the top of soil is a vertical stress of $\sigma'_v = 200$ kPa, and a horizontal stress of $\sigma'_h = 120$ kPa in both the lateral and in-plane directions. The pre-consolidation pressure, p'_c at a point in the soil domain was defined by assuming the soil is normally consolidated, so the current yield locus passes through the initial stress points. Consequently,

$$(2) \quad p'_c = \frac{q_0^2}{M^2 p'_0} + p'_0$$

where p'_0 and q_0 are the initial effective mean stress and deviatoric stress, respectively, at that depth and M is the slope of the critical state line in p - q space. The initial void ratio, e_0 , at a point is defined as

$$(3) \quad e_0 = e_1 - \kappa \ln p'_0 - (\lambda - \kappa) \ln p'_c$$

where

$$(4) \quad e_1 = e_{cs} + (\lambda - \kappa) \ln(2)$$

with e_{cs} being the void ratio at 1 kPa mean effective stress on the critical state line, λ the slope of the virgin consolidation line and the critical state line, and κ the slope of the swelling line.

The interface between the pipe and the soil was assumed to be fully smooth (mobilizing zero shear stress during tangential movement) or fully rough (with adjacent pipe and soil nodes being tied). The pore-water pressure distribution was initially hydrostatic.

Effect of loading rate on penetration resistance

Fully coupled consolidation stress analyses following the RITSS approach were performed. The pipe penetrated to an embedment of 50% of its diameter with different velocities, v , and thus different values of the nondimensional velocity, vD/c_v . The consolidation coefficient, c_v , can be determined from

$$(5) \quad c_v = \frac{k}{m_v \gamma_w}$$

where k is the permeability, m_v is the volume compressibility, and γ_w is the unit weight of water. The virgin compressibility in the Cam clay model is expressed as

$$(6) \quad m_v = \frac{\lambda}{(1 + e_0)p'_0}$$

A wide range of values of vD/c_v from a very high velocity ($vD/c_v = 100$) down to the lowest velocity corresponding to $vD/c_v (= 0.025)$ were considered. The highest velocity means that negligible excess pore-water pressure can dissipate and undrained conditions are approached. In contrast, slower velocities of the pipe lead to a partially drained and ultimately a fully drained response. This brackets the range of conditions expected to occur in practice. For very low-permeability clayey soils, the penetration response is most likely to be undrained; with increasing silt content, a par-

tially drained response will occur; and fully drained penetration will occur in coarser soils.

Figure 3 shows the variation of normalized penetration resistance with depth for a smooth pipe–soil interface, and Fig. 4 shows the same results for a rough pipe–soil interface. The resistance force is normalized using the undrained shear strength, s_{u0} , at the pipe invert obtained from the MCC parameters for K_0 consolidated soil. For the plane strain conditions relevant here, the undrained shear strength, s_u , may be expressed as (Wroth 1984)

$$(7) \quad s_u = \frac{2}{\sqrt{3}} \frac{\sin \phi_{tc}}{2a} \left(\frac{a^2 + 1}{2} \right)^\Lambda \sigma'_v$$

where

$$(8) \quad a = \frac{3 - \sin \phi_{tc}}{2(3 - 2 \sin \phi_{tc})} \quad \text{and} \quad \Lambda = \frac{\lambda - \kappa}{\lambda}$$

For the parameters listed in Table 1, the initial undrained shear strength obtained was 57.2 kPa at the mudline and 64.4 kPa at the bottom of the mesh.

At the two highest penetration rates, the resistance profiles are similar, suggesting that fully undrained conditions are almost reached. This is confirmed by the results of an analysis performed using the same numerical technique, but with the Tresca soil model and equivalent undrained shear strength. These results are also shown in Figs. 3 and 4. Excellent agreement is evident, indicating that the fastest cases correspond to practically undrained conditions.

At lower pipe velocities, the penetration resistances are higher (Fig. 3). Numerical convergence problems were observed for a very low penetration rate simulating fully drained conditions. However, there are negligible differences in the resistance responses for $vD/c_v = 0.1$ and $vD/c_v = 0.025$ or 0.05. This indicates that pipe velocities corresponding to $vD/c_v = 0.1$ or lower lead to essentially fully drained resistance, even though small excess pore pressures are still present. The contours of excess pore-water pressure normalized by the bearing pressure ($q = V/D$) at $w/D = 0.5$ for the highest and lowest penetration rates (nominally undrained and drained cases) for smooth and rough pipes are shown in Fig. 5. For the lowest pipe penetration rate, the excess pore pressure generated beneath the pipe is much less compared to that for the undrained cases.

The ratio between the drained and undrained penetration resistance increases with pipe embedment. Compared to the smooth case, more resistance is observed at a particular embedment level for the rough pipe–soil interface. However, the relative increase in resistance from the fully undrained to the fully drained case is lower in the case of rough pipe. At the embedment level of $w/D = 0.5$, for the smooth pipe, a 72% increase in resistance is observed from the fully undrained condition to the fully drained condition, whereas a difference of approximately 48% is found for the rough pipe.

To illustrate the transition between drained and undrained conditions, the resistance (V) for a particular pipe velocity is normalized by the undrained resistance ($V_{\text{undrained}}$) at that depth and plotted against the nondimensional velocity. Figure 6 shows the resulting “backbone” curves at different embedment levels for smooth and rough pipes. For $vD/c_v \leq 0.1$, the resistance is independent of velocity and the response is essentially drained. For $vD/c_v \geq 100$, the response stabilizes and the response is fully undrained. The nondimensional velocities in between these limits correspond to partially drained behaviour. The backbone curves for smooth and rough pipes can be fitted to a simple hyperbolic equation of the form

Fig. 3. Normalized penetration resistances with embedment for different pipe velocities (smooth pipe).

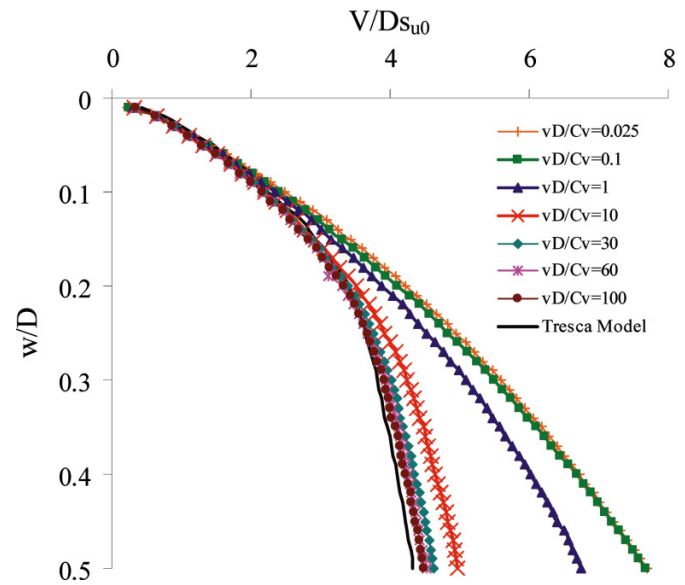
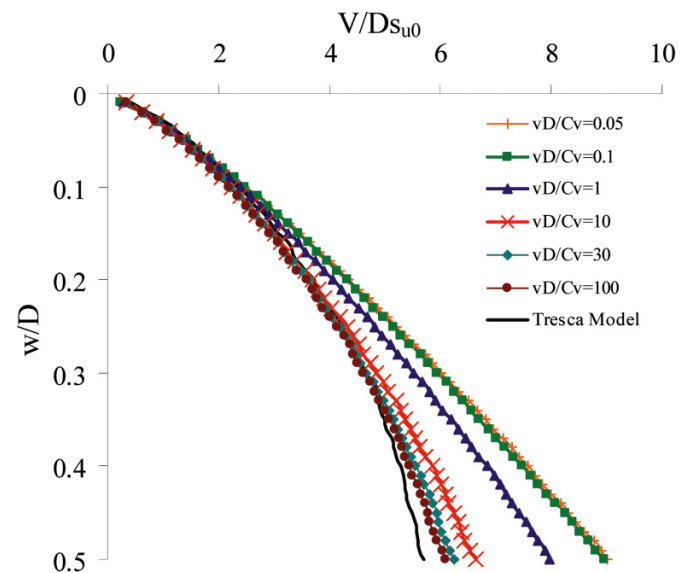


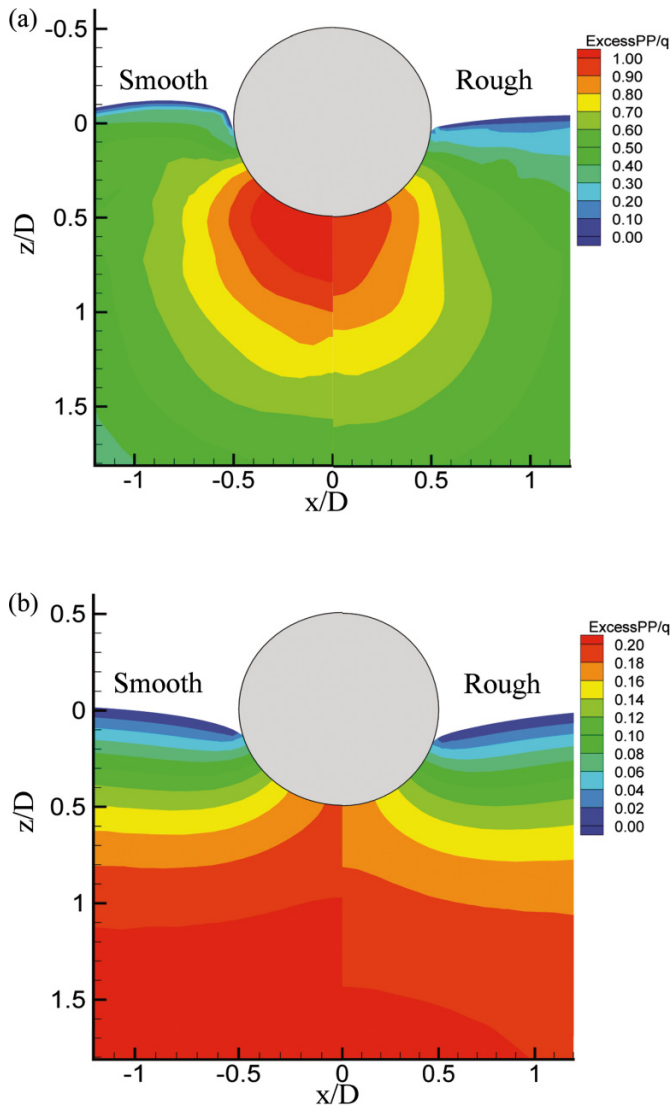
Fig. 4. Normalized penetration resistances with embedment for different pipe velocities (rough pipe).



$$(9) \quad \frac{V}{V_{\text{undrained}}} = a + \frac{b}{1 + [(vD/c_v)/(vD/c_v)_{50}]^c}$$

where $(vD/c_v)_{50}$ is the normalized penetration rate that gives a response midway between the drained and undrained limits. For higher values of vD/c_v , i.e., for undrained cases, $V/V_{\text{undrained}}$ tends to unity, so the value of parameter “a” is always 1. The parameter “b” controls the drained limit of the backbone curve as $vD/c_v \rightarrow 0$. The quantities “c” and $(vD/c_v)_{50}$ were varied to obtain best-fit curves for all embedment levels for smooth as well as rough pipes. It was found that values of $c = 1$ and $(vD/c_v)_{50} = 2$ gave reasonably fitting curves for all initial embedment and smooth and rough pipes. The parameter “b” depends on the initial embedment level and can be expressed as a power law function of the embedment depth. For a smooth pipe

Fig. 5. Contours of excess pore-water pressure normalized by penetration resistance: (a) $vD/c_v = 100$; (b) $vD/c_v = 0.1$.



$$(10) \quad b \sim 1.45(w/D)$$

and for a rough pipe

$$(11) \quad b \sim 0.92(w/D)^{0.9}$$

For comparison, a number of analyses were run for a low surcharge of 1 kPa at the top surface for the smooth pipe. For the case of 1 kPa surcharge, the value of c_v varies considerably with depth. Hence, while calculating nondimensional velocity vD/c_v , c_v was chosen at depth of $1D$. Figure 7 shows the backbone curves for different embedments for 1 kPa surcharge. The $V/V_{\text{undrained}}$ ratios are generally higher at the drained end for this case. However, for embedment levels of $w/D = 0.2$ or more, the backbone curves are closer to each other compared to the 200 kPa case. This indicates that for 1 kPa surcharge, the $V/V_{\text{undrained}}$ ratio increases less as the pipe penetrates deeper.

Consolidation settlement

At different levels of vertical embedment, i.e., at $w/D = 0.1, 0.2, 0.3, 0.4,$ and 0.5 , the consolidation settlement behaviour was also studied. The excess pore-water pressure generated during the undrained

pipe penetration was allowed to dissipate under the full penetration resistance load experienced at the respective embedment level. The settlement (Δw) variations for different embedment levels are shown in Fig. 8, as a function of nondimensional time factor $T (= c_v t/D^2)$, for initial penetrations at speeds of $vD/c_v = 0.1$ (drained) and 100 (undrained). For the (nominally) drained penetration case, the pore-water pressure is partially dissipated during penetration and hence the subsequent consolidation settlement should be less than for the undrained case. However, this is more than compensated for by the greater resistance experienced during drained penetration, and thus higher loads applied during the consolidation phase. If the same load were to be applied during consolidation, the consolidation settlement would indeed be much less following drained penetration compared to the undrained case. This phenomenon is illustrated in Fig. 9 for the smooth pipe, where for the drained case the loads were reduced (following penetration, prior to consolidation) to the same as for the corresponding undrained case.

It may be seen that the overall time-scale of consolidation is the same, regardless of the degree of consolidation during initial penetration. The time-scale for consolidation settlement is essentially dictated by the far-field pore pressures, and is nearly two orders of magnitude greater than for pore pressure dissipation adjacent to the pipe (Chatterjee et al. 2012c).

Pore water pressure dissipation time history

The axial and lateral resistance of the pipeline are affected significantly by the degree of consolidation following installation. This may be characterized by the average excess pore pressure around the embedded pipe perimeter (Δu_{av}), normalized by the initial average value ($\Delta u_{\text{av,init}}$), as plotted for different initial embedment levels against the nondimensional time T in Fig. 10. The consolidation response can be fitted by a simple hyperbolic equation of the form

$$(12) \quad \frac{\Delta u_{\text{av}}}{\Delta u_{\text{av,init}}} = \frac{1}{1 + (T/T_{50})^m}$$

where T_{50} is the nondimensional time required for 50% dissipation of the average excess pore pressure. The values of T_{50} and index “ m ” for different embedment levels are tabulated in Table 2. The T_{50} values from the present study are less than those published previously for elastic soil (Gourvenec and White 2010), indicating faster dissipation (Table 3).

Lateral breakout resistance

Background

After the pipe is partially embedded into the seabed, it can be displaced laterally in response to internal temperature and pressure, or as a result of external hydrodynamic loading. The breakout resistance, i.e., the peak lateral resistance experienced by the pipe as it displaces laterally, depends strongly on the strength of the surrounding soil. The direction of the pipe movement at this stage also depends on the weight of the pipe relative to the strength of the seabed (although noting that this will not be simulated well in the present study, because of the artificially high shear strength resulting from the surcharge of 200 kPa).

The available solutions for breakout resistance in the literature are mainly confined to undrained breakout, with the strength of the surrounding soil being unaffected by consolidation. In reality, there is always a significant duration between pipe laying and operation. During this time, consolidation of the soil below and around the pipe can occur under the weight of the pipe and contents. Dissipation of positive excess pore-water pressure leads to an increase in the shear strength of the soil near the pipe. So, before breakout occurs, the strength distribution around the pipe is altered, and the breakout resistance is potentially raised.

Fig. 6. Backbone curves for different initial embedment levels: (a) smooth interface; (b) rough interface.

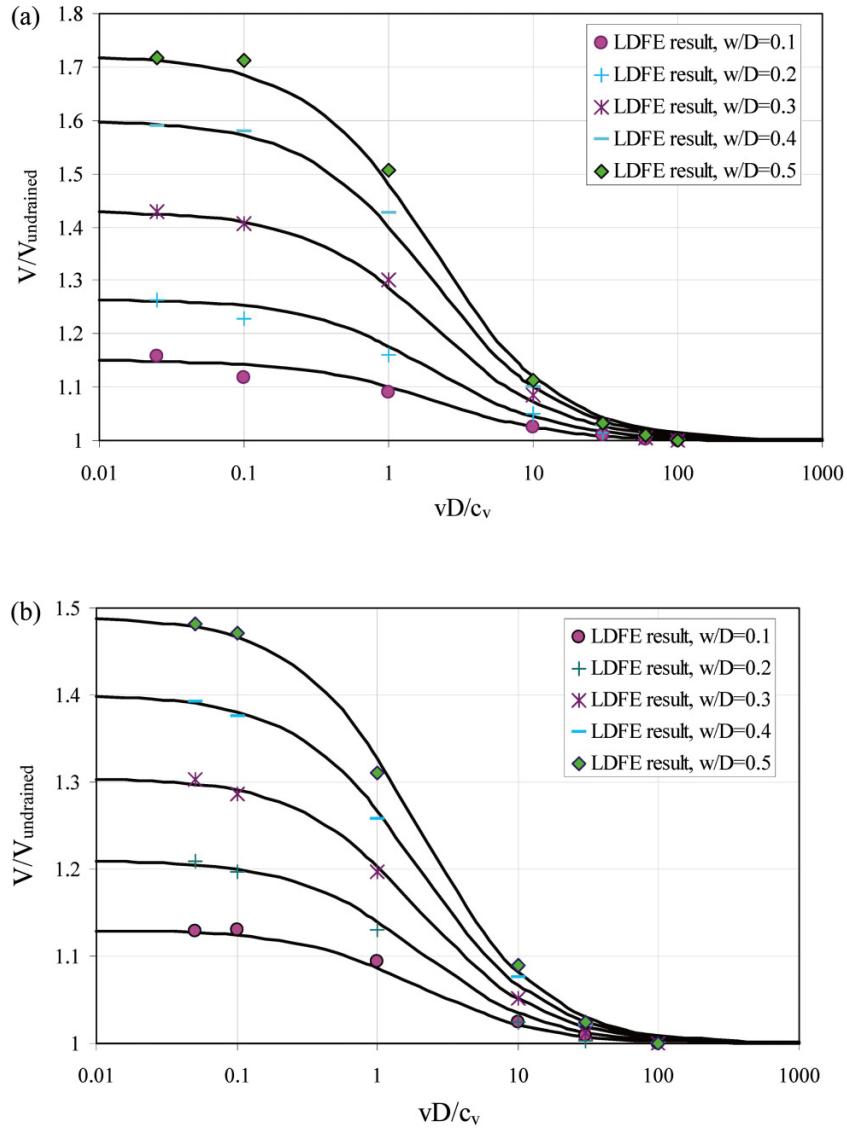


Fig. 7. Backbone curves for different initial embedment levels (smooth pipe, 1 kPa surcharge).

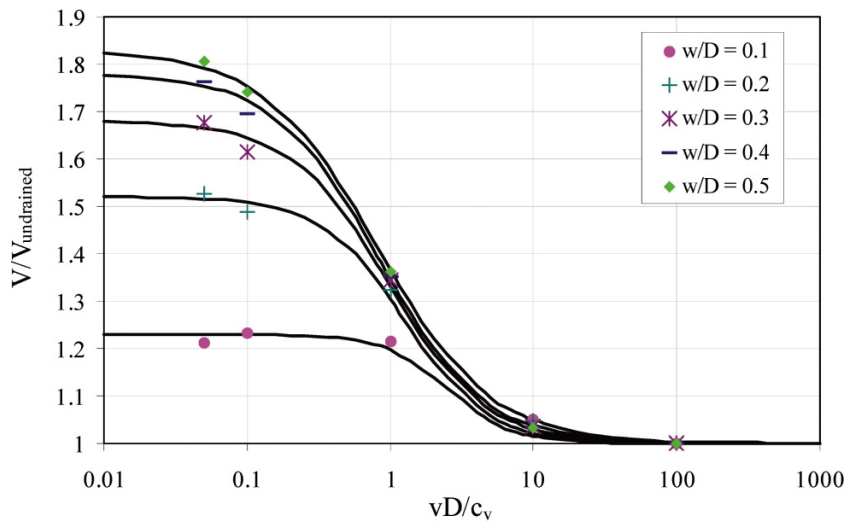


Fig. 8. Pipe settlements with time for different initial embeddings and pipe velocities: (a) smooth interface; (b) rough interface.

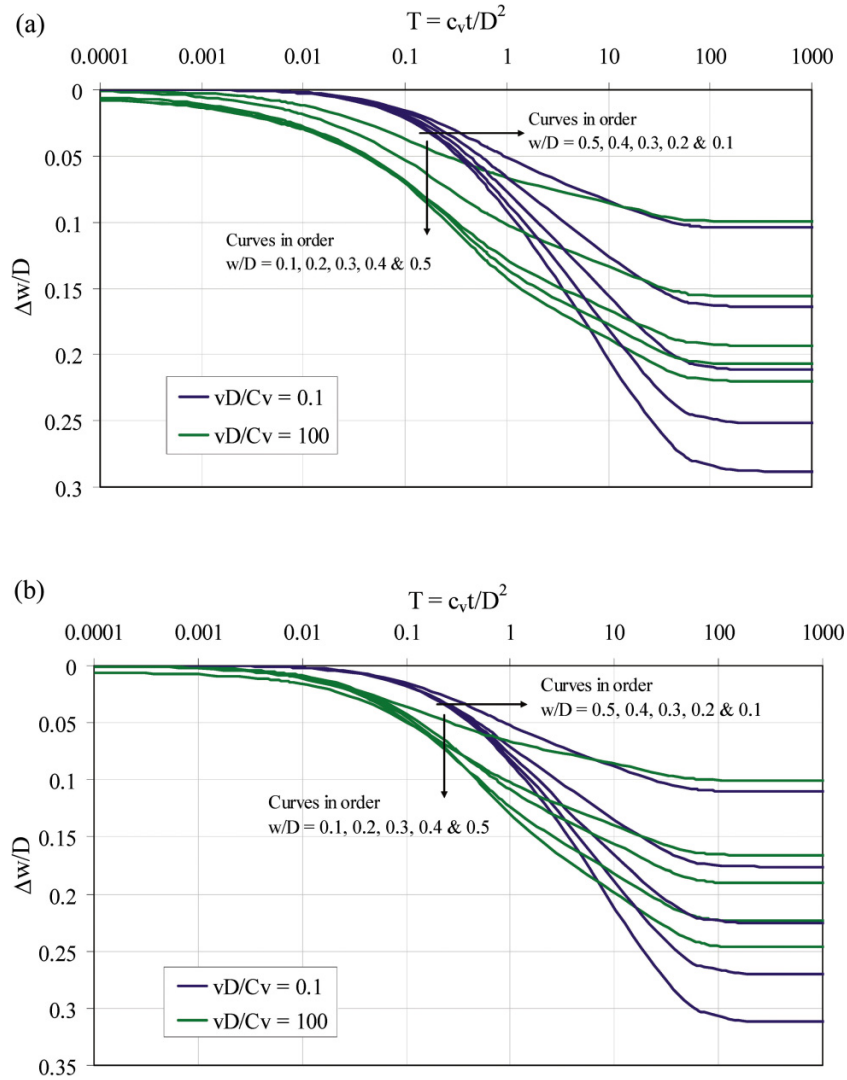


Fig. 9. Consolidation settlements following penetration at different speeds under the same consolidation load (smooth pipe).

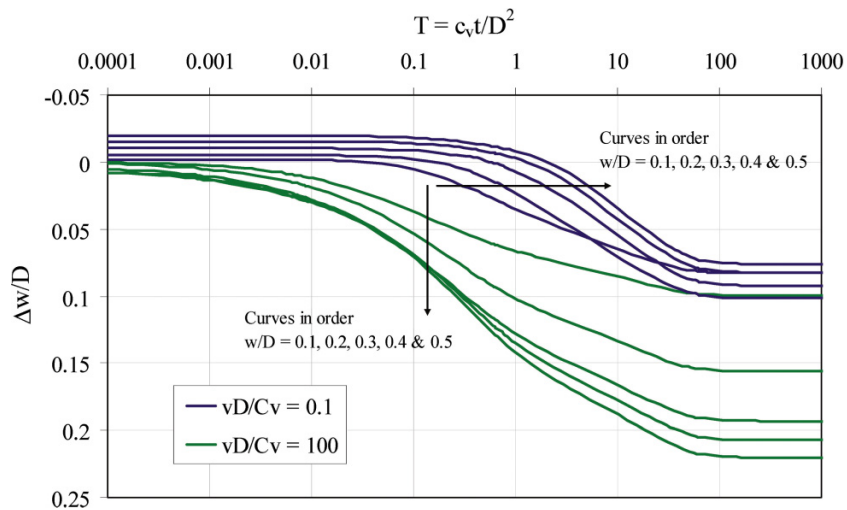


Fig. 10. Dissipation of excess pore-water pressure with nondimensional time T .

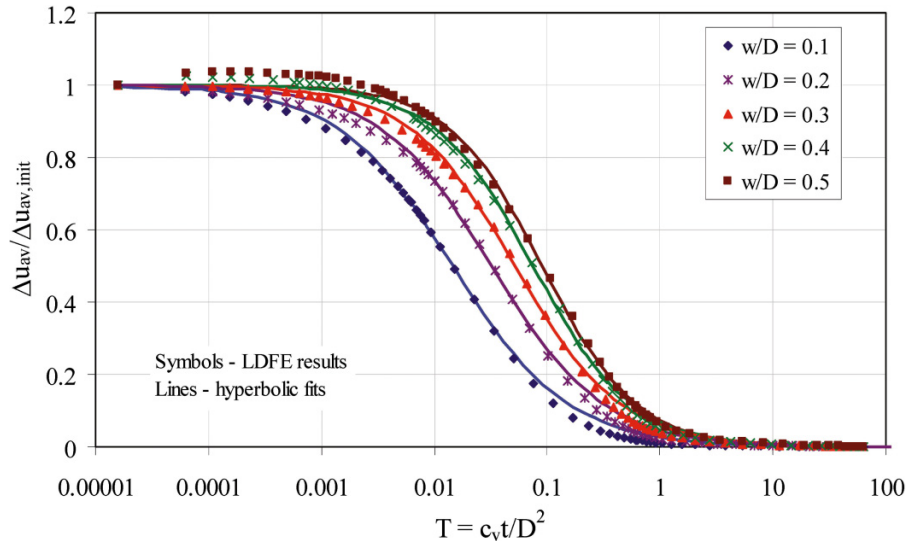


Table 2. Values of T_{50} and constant “ m ” of hyperbolic fits.

Initial embedment ratio, w/D	T_{50}	m
0.1	0.015	0.85
0.2	0.032	0.88
0.3	0.052	0.93
0.4	0.075	1.00
0.5	0.090	1.05

Table 3. Comparison of values of T_{50} from the present study and elastic solution (Gourvenec and White 2010).

Initial embedment ratio, w/D	T_{50}	
	Present study	Gourvenec and White (2010)
0.1	0.015	0.018
0.2	0.032	0.042
0.3	0.052	0.068
0.4	0.075	0.096
0.5	0.090	0.121

The breakout resistance depends on the load path in V - H space, so the best basis for describing the potential breakout resistance is to determine the yield envelope in V - H space. In this study, yield envelopes in V - H load space have been evaluated by numerical analyses, for a smooth pipe-soil interface only, for two conditions: (i) immediately after undrained penetration (referred to as unconsolidated, undrained) and (ii) after full consolidation following undrained penetration (referred to as consolidated, undrained). In both cases, the pipeline movement during penetration and breakout was at rate corresponding to a normalized velocity of 100, giving nominally undrained conditions. The failure loads in V - H space were obtained by displacing the pipe by 10% of its diameter in different directions.

Unconsolidated undrained yield envelopes

Firstly, the unconsolidated undrained case is considered. The limiting values of vertical and horizontal resistances have been normalized by the initial undrained shear strength at that depth. The resulting yield envelopes in V - H space for $w/D = 0.1, 0.2, 0.3, 0.4,$ and 0.5 are shown in Fig. 11. These results exceed the equiva-

lent results presented by Randolph and White (2008) by typically 15% because the latter analyses considered only a flat seabed (with the pipe washed into place) and ignored the self-weight of the soil. Buoyancy effects due to soil self-weight are minimal in the present study, because of the high shear strength. However, the berm of soil displaced during penetration in the present study results in greater soil resistance. Merifield et al. (2009) reported results of FE analyses using a Tresca model and also considered the effects of soil berms on the vertical penetration and horizontal breakout resistances. Results from that study for pure vertical and pure horizontal pipe movements are also shown in Fig. 11. Their results are close to the present study, with a maximum error below 9% (except for $w/D = 0.1$). The close agreement confirms the correct operation of the MCC soil model for fully undrained conditions.

Consolidated undrained yield envelopes

Figure 12 shows the consolidated undrained yield envelopes for different initial embedment levels after full pore pressure dissipation. To make a comparison between the unconsolidated and consolidated cases, results for two initial embedment levels of $w/D = 0.1$ and 0.5 are plotted in Fig. 13. The growth in the size of the yield envelope was 66% for pure vertical movement for both $w/D = 0.1$ and 0.5 . For pure horizontal movement, the horizontal resistance is 138% greater for the consolidated case for $w/D = 0.1$, whereas the increase is 83% for $w/D = 0.5$.

Contours of the strength increase compared to the original undrained shear strength at the embedment level of $w/D = 0.5$ ($w/D \sim 0.75$ following consolidation) are shown in Fig. 14. The consolidated strength reaches 2.1 times the original strength just beneath the pipe. The increase in strength is greatest beneath the pipe — within the soil that controls the response to vertical loading — and a lower increase in strength is evident to the side of the pipe — within the soil that controls the response to horizontal loading.

Fitted functions for yield envelopes

The FE results shown in Figs. 11 and 12, which form the undrained yield envelopes, can be fitted by an equation with the form of a distorted ellipse

$$(13) \quad \frac{H}{D s_{u0}} = f\beta \left(\frac{V}{D s_{u0}} \right)^{\beta_1} \left(\frac{V_{\max}}{D s_{u0}} - \frac{V}{D s_{u0}} \right)^{\beta_2}$$

where

Fig. 11. Yield envelopes for different initial embeddings for unconsolidated undrained case (smooth pipe).

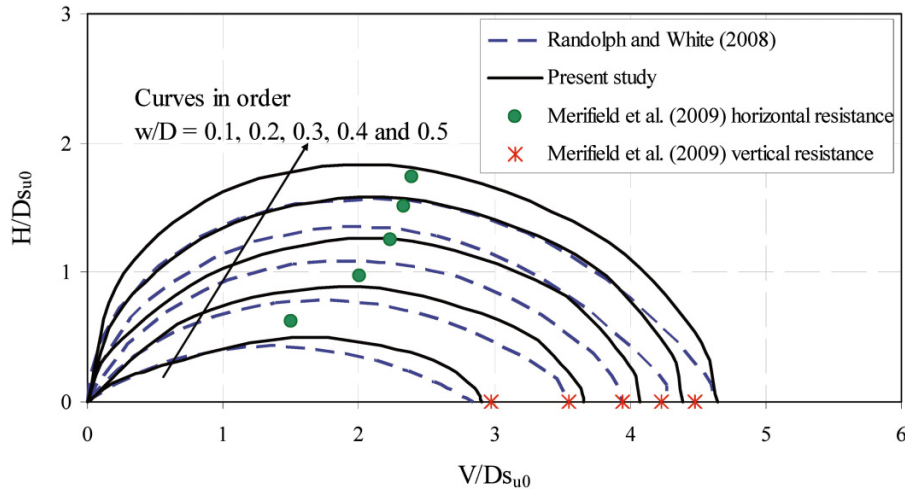


Fig. 12. Yield envelopes for different initial embeddings for consolidated undrained case (smooth pipe).

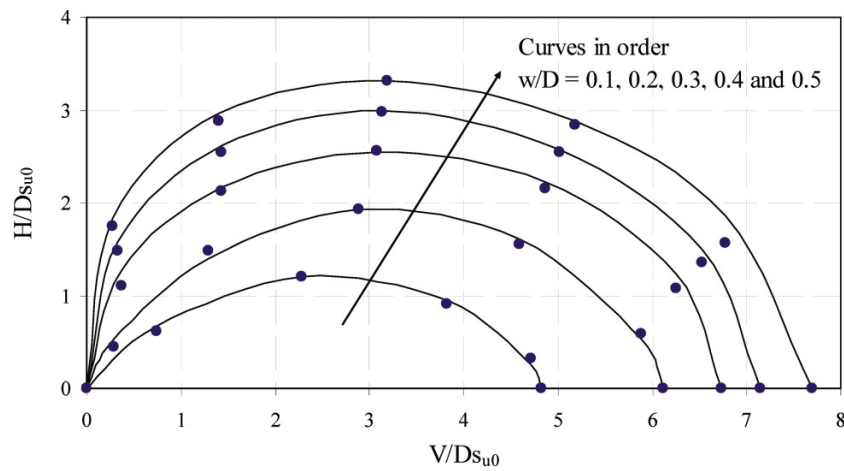
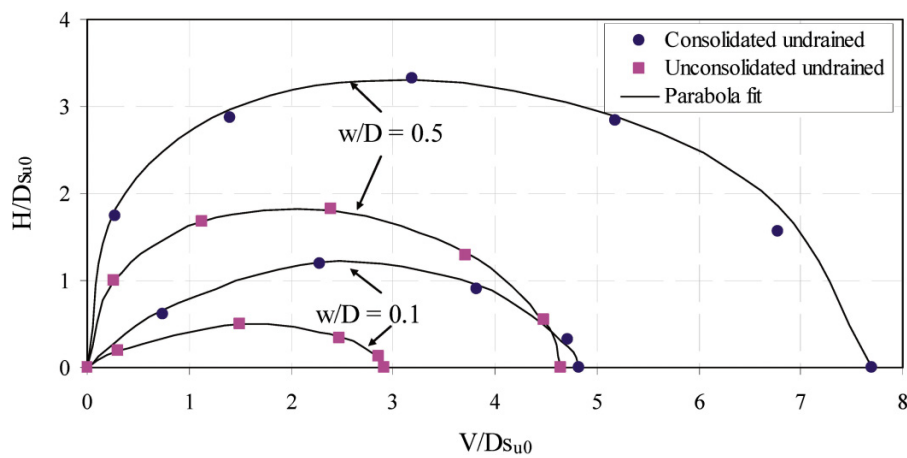


Fig. 13. Comparison of yield envelopes for unconsolidated undrained and consolidated undrained conditions for w/D = 0.1 and 0.5 (smooth pipe).



$$(14) \quad \beta = \frac{(\beta_1 + \beta_2)^{(\beta_1 + \beta_2)}}{\beta_1^{\beta_1} \beta_2^{\beta_2}}$$

Here, the parameters β_1 and β_2 skew the ellipse and f is a factor determining the aspect ratio of the ellipse; V_{max} is the undrained

resistance under pure vertical loading. The values of the parameters f , β_1 , and β_2 for different initial embedment levels and unconsolidated and consolidated cases are tabulated in Table 4. The values of normalized V_{max} versus normalized embedment for unconsolidated and consolidated cases are plotted in Fig. 15. These responses can be fitted by a simple power law equation of the form

Fig. 14. Contours of ratios of consolidated shear strength to the original shear strength (smooth pipe, 200 kPa surcharge).

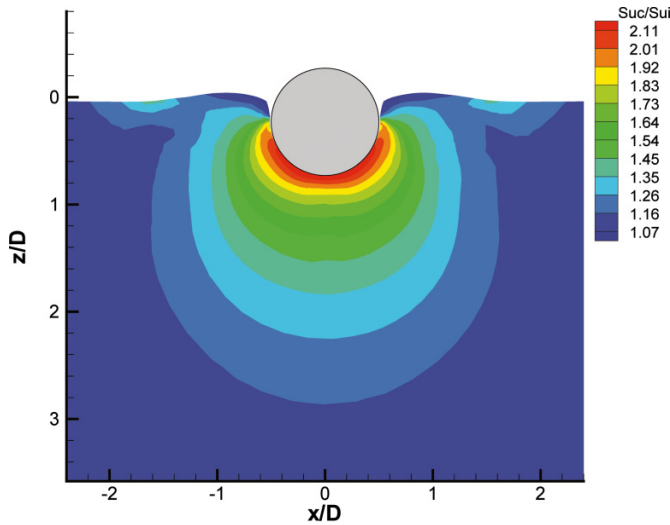
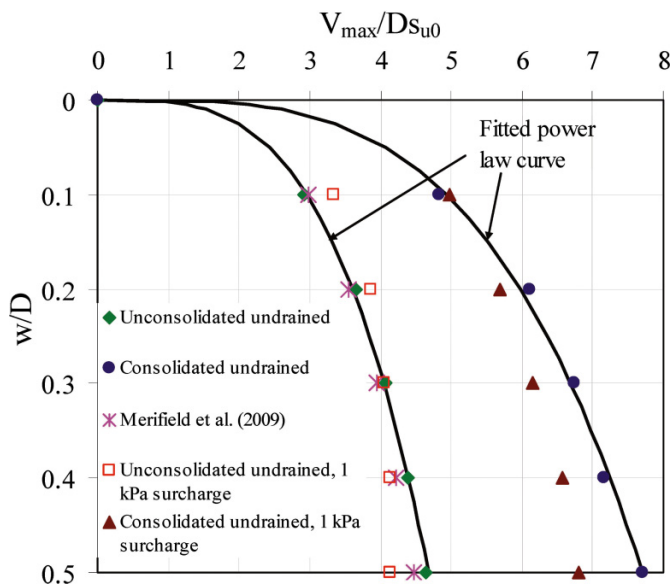


Table 4. Values of f , β_1 , and β_2 for unconsolidated and consolidated conditions.

Initial embedment ratio, w/D	Unconsolidated undrained			Consolidated undrained		
	f	β_1	β_2	f	β_1	β_2
0.1	0.14	0.83	0.64	0.26	0.81	0.7
0.2	0.16	0.70	0.65	0.32	0.75	0.7
0.3	0.22	0.65	0.61	0.39	0.46	0.52
0.4	0.31	0.53	0.58	0.47	0.41	0.53
0.5	0.37	0.45	0.59	0.55	0.35	0.53

Fig. 15. Maximum vertical penetration resistances for unconsolidated undrained and consolidated undrained conditions (smooth pipe).



$$(15) \quad \frac{V_{max}}{D S_{u0}} = a \left(\frac{w}{D} \right)^b$$

Coefficients “ a ” and “ b ” for unconsolidated and consolidated cases are listed in Table 5. In the same figure (Fig. 15), results from

Table 5. Power law fit coefficient “ a ” and “ b ” for unconsolidated and consolidated conditions.

Conditions	a	b
Unconsolidated undrained	5.7	0.29
Consolidated undrained	9.3	0.28

Merifield et al. (2009) are also plotted for comparison with the unconsolidated undrained case and show good agreement.

Results for 1 kPa surcharge are also shown for the unconsolidated and consolidated cases in Fig. 15. There are considerable buoyancy effects in the overall resistance for the 1 kPa surcharge case, unlike the 200 kPa case. The maximum penetration resistances for the 1 kPa surcharge case that are plotted in Fig. 15 are the geotechnical capacity after correction for buoyancy.

Concluding remarks

The consolidation of soil around deep-water pipelines is an important phenomenon to consider for correct prediction of pipe-soil interactions. A large deformation finite element (LDFE) methodology combined with the modified Cam clay (MCC) plasticity soil model was developed for this study to explore the coupled consolidation behaviour beneath partially embedded seabed pipelines.

The penetration resistance during embedment of the as-laid pipes depends markedly on the rate of penetration, with the resistance increasing with the degree of consolidation during penetration. Results have been presented for both smooth and rough pipe-soil interfaces for normalized embedment, w/D , from 0.1 to 0.5. Up to 72% increase in resistance was observed from fully undrained to fully drained conditions.

Backbone curves, i.e., penetration resistance versus nondimensional velocities for smooth and rough pipes, have also been presented. From these curves, fully drained conditions pertain for $vD/c_v = 0.1$ or lower, while undrained conditions pertain for $vD/c_v = 100$ or higher. The backbone curves are presented in terms of simple hyperbolic equations fitted to the LDFE results.

The strength of the soil beneath and around the pipe, and hence the breakout resistance, depends on the extent to which consolidation occurs following penetration. The resulting changes in the size and shape of the undrained yield envelopes were shown to be significant for initially normally consolidation conditions. It was found that the vertical bearing capacities were increased by 66% for embedments of $w/D = 0.1$ and 0.5, if consolidation under the full vertical bearing capacity was permitted following penetration. The resistances during pure horizontal movement were increased by 138% and 83% for $w/D = 0.1$ and 0.5, respectively.

These effects of consolidation — which strongly influence the stability of an on-bottom pipeline — are important to consider in design to provide realistic prediction of pipe-soil interaction forces. In this study, the consolidation analyses were performed under the full bearing capacity, although in practice the applied load may be less during this phase, leading to a smaller strength increase. The resulting increases in $V-H$ capacity presented here should therefore be taken as upper bounds to the potential range of behaviour.

Acknowledgements

This work forms part of the activities of the Centre for Offshore Foundation Systems (COFS) at The University of Western Australia, currently supported as a node of the Australian Research Council Centre of Excellence for Geotechnical Science and Engineering, and by The Lloyd's Register Foundation. The second and third authors acknowledge respective support through the ARC Future Fellowship and Discovery programs as well as, for the second author, from Shell Australia.

References

- AtkinsBoreas 2008. SAFEBUCK JIP – Safe design of pipelines with lateral buckling. Design Guideline. AtkinsBoreas. Report No. BR02050/SAFEBUCK/C.
- Aubeny, C.P., Shi, H., and Murff, J.D. 2005. Collapse loads for a cylinder embedded in trench in cohesive soil. *International Journal of Geomechanics*, **5**(4): 320–325. doi:10.1061/(ASCE)1532-3641(2005)5:4(320).
- Bruton, D.A.S., White, D.J., Carr, M., and Cheuk, C.Y. 2008. Pipesoil interaction during lateral buckling and pipeline walking – the Safebuck JIP. *In Proceedings of the Offshore Technology Conference*, Houston, Tex., 5–8 May 2008. Offshore Technology Conference, Richardson, Tex. OTC 19589.
- Cardoso, C.O., and Silveira, R.M.S. 2010. Pipe–soil interaction behavior for pipelines under large displacements on clay soils: a model for lateral residual friction factor. *In Proceedings of the Offshore Technology Conference*, Houston, OTC 20767.
- Chatterjee, S., Randolph, M.F., and White, D.J. 2012a. The effects of penetration rate and strain softening on the vertical penetration resistance of seabed pipelines. *Géotechnique*, **62**(7): 573–582. doi:10.1680/geot.10.P.075.
- Chatterjee, S., White, D.J., and Randolph, M.F. 2012b. Numerical simulations of pipe-soil interaction during large lateral movements on clay. *Géotechnique*, **62**(8): 693–705. doi:10.1680/geot.10.P.107.
- Chatterjee, S., Yan, Y., Randolph, M.F., and White, D.J. 2012c. Elastoplastic consolidation beneath shallowly embedded offshore pipelines. *Géotechnique Letters*, **2**: 73–79. doi:10.1680/geolett.12.00031.
- Cheuk, C.Y., White, D.J., and Bolton, M.D. 2007. Large-scale modelling of soil-pipe interaction during large amplitude movements of partially-embedded pipelines. *Canadian Geotechnical Journal*, **44**(8): 977–996. doi:10.1139/T07-037.
- Dassault Systèmes. 2011. Abaqus analysis users' manual. Simula Corp, Providence, R.I.
- Dingle, H.R.C., White, D.J., and Gaudin, C. 2008. Mechanisms of pipe embedment and lateral breakout on soft clay. *Canadian Geotechnical Journal*, **45**(5): 636–652. doi:10.1139/T08-009.
- Ghosh, S., and Kikuchi, N. 1991. An arbitrary Lagrangian-Eulerian finite element method for large deformation analysis of elastic-viscoplastic solids. *Computer Methods in Applied Mechanics and Engineering*, **86**(2): 127–188. doi:10.1016/0045-7825(91)90126-Q.
- Gourvenec, S.M., and White, D.J. 2010. Elastic solutions for consolidation around seabed pipelines. *In Proceedings of the Offshore Technology Conference*, Houston, Tex. OTC 20554.
- Hu, Y., and Randolph, M.F. 1998a. A practical numerical approach for large deformation problems in soil. *International Journal for Numerical and Analytical Methods in Geomechanics*, **22**(5): 327–350. doi:10.1002/(SICI)1096-9853(199805)22:5<327::AID-NAG920>3.0.CO;2-X.
- Hu, Y., and Randolph, M.F. 1998b. H-adaptive FE analysis of elasto-plastic non-homogeneous soil with large deformation. *Computers and Geotechnics*, **23**(1–2): 61–83. doi:10.1016/S0266-352X(98)00012-3.
- Krost, K., Gourvenec, S.M., and White, D.J. 2011. Consolidation around partially embedded seabed pipelines. *Géotechnique*, **61**(2): 167–173. doi:10.1680/geot.8.T.015.
- Merifield, R., White, D.J., and Randolph, M.F. 2008. The ultimate undrained resistance of partially embedded pipelines. *Géotechnique*, **58**(6): 461–470. doi:10.1680/geot.2008.58.6.461.
- Merifield, R.S., White, D.J., and Randolph, M.F. 2009. Effect of surface heave on response of partially embedded pipelines on clay. *Journal of Geotechnical and Geoenvironmental Engineering*, **135**(6): 819–829. doi:10.1061/(ASCE)GT.1943-5606.0000070.
- Randolph, M.F., and White, D.J. 2008. Upper-bound yield envelopes for pipelines at shallow embedment in clay. *Géotechnique*, **58**(4): 297–301. doi:10.1680/geot.2008.58.4.297.
- Roscoe, K.H., and Burland, J.B. 1968. On the generalised stress-strain behaviour of 'wet clay'. *In Engineering plasticity*. Cambridge University Press.
- Schofield, A., and Wroth, C.P. 1968. *Critical state soil mechanics*. McGraw-Hill, New York.
- Senthilkumar, M., Kodikara, J., and Rajeev, P. 2011. Numerical modelling of vertical load displacement behaviour of offshore pipeline using coupled analysis. *Pan Am CGS Geotechnical Conference*, Toronto, Ont.
- Stewart, D.P. 1992. Lateral loading of piled bridge abutments due to embankment construction. Ph.D. thesis, The University of Western Australia.
- Wang, D., White, D.J., and Randolph, M.F. 2010. Large-deformation finite element analysis of pipe penetration and large-amplitude lateral displacement. *Canadian Geotechnical Journal*, **47**(8): 842–856. doi:10.1139/T09-147.
- White D.J., and Cheuk, C.Y. 2005. SAFEBUCK JIP: Lateral pipe-soil interaction: Data review. Report to Boreas Consultants (SAFEBUCK JIP), ref. SC-CUTS-0502-R02.
- White, D.J., and Cheuk, C.Y. 2009. SAFEBUCK JIP: Pipe-soil interaction models for lateral buckling design: Phase IIA data review. Report to Boreas Consultants (SAFEBUCK JIP), UWA report GEO 09497.
- Wroth, C.P. 1984. The interpretation of in situ soil tests. *Géotechnique*, **34**(4): 449–489. doi:10.1680/geot.1984.34.4.449.
- Zienkiewicz, O.C., and Zhu, J.Z. 1992. The superconvergent patch recovery and a posteriori error estimates. Part 1: The recovery technique. *International Journal of Numerical Methods in Engineering*, **33**(7): 1331–1364. doi:10.1002/nme.1620330702.